Precision frequency measurements with polarized ^{3}He, ^{21}Ne, and ^{129}Xe atoms

T. E. Chupp, E. R. Oteiza, J. M. Richardson, and T. R. White
Department of Physics and Lyman Laboratory of Physics, Harvard University, Cambridge, Massachusetts 02138
(Received 13 October 1987)

We present the principles, applications, and performance of new techniques developed to measure the frequency spectrum of freely precessing polarized noble-gas atoms. The noble-gas polarization technique of spin exchange with laser optically pumped Rb enables us to simultaneously polarize several species (^{3}He, ^{21}Ne, and ^{129}Xe). With signal-to-noise ratios of 10^4, the free precession frequencies are determined with a precision of less than 10^{-6} Hz out of 10^3 Hz in 1024 sec. The technique will be applied to determine frequency shifts due to dipole couplings to applied fields and quadrupole splittings due to local Lorentz-invariance-violating spatial anisotropy. In all cases, the frequencies of two or more species are measured simultaneously in order to provide magnetometry for increased precision and to provide measurement and cancellation of systematic effects.

I. INTRODUCTION

The technique of noble-gas-atom polarization by spin exchange with laser optically pumped Rb vapor can now produce nearly 100% polarized samples of ^{3}He (Refs. 1 and 2) and ^{21}Ne (Ref. 3) as well as heavier noble gases Kr (Ref. 4), Xe (Refs. 4 and 5), and Rn.[6] For ^{3}He and ^{21}Ne, the spin-exchange coupling to the Rb or K is sufficiently weak that more than 10^{21} atoms cm^{-3} can be polarized without reducing the alkali-metal polarization. Samples with 10^{19} polarized noble-gas atoms produce up to 10^{-4}-G magnetization, and the freely precessing atoms have observed coherence times of up to 2000 s. The ratio of signal to noise for a 1024-s measurement is greater than 10^4, and it is therefore possible to determine the precession frequency with a precision better than 10^{-6} Hz. In order to realize this precision, the effective magnetic field noise must be suppressed to less than 10^{-10} G. This is achieved by using two or more species (e.g., ^{3}He and ^{21}Ne), one of which is used to track the magnetic field.

We are using these samples to measure the precession frequency spectrum of the atoms as they interact with applied fields and a possible local Lorentz invariance violating anisotropy of space. The dipole interaction with the applied magnetic field is used to determine atomic magnetic dipole moments; the dipole interaction with simultaneously applied magnetic and electric fields is used to search for permanent atomic electric dipole moments; the quadrupole splitting of ^{21}Ne NMR lines is used to study local Lorentz invariance. The ability to polarize and simultaneously measure the precession frequency spectra of two or more species also provides a handle on systematic effects that are present in these kinds of experiments.

The principles of noble-gas polarization are described in detail in Ref. 1–6. In particular, Ref. 2 details our current understanding of ^{3}He polarization and Ref. 5 discusses ^{129}Xe polarization. In this paper, the apparatus and techniques are presented along with the principles of analysis for each experiment.

II. APPARATUS

We first present a description of the apparatus and its operation. The major components, shown in Fig. 1, are the laser system, the cell or bottle containing the noble gases, buffer gasses, and alkali metal, the precision solenoid, the NMR coils, and the signal processing electronics.

The laser light for optical pumping is currently provided by LD700 dye pumped by the red lines of a Kr^+ laser. The dye laser is a standing-wave, multimode laser with a three-element birefringent filter. The laser linewidth is 30 GHz, measured with a scanning monochrometer. The Rb $D1$ resonance line has a pressure broadened width of 18 GHz at 1 atm total pressure (3×10^{19} cm^{-3}). At 795 nm, the Rb-$D1$ resonance wavelength, up to 1 W is available. The linearly polarized laser light is circularly polarized with a $\lambda/4$ plate after expansion by a telescope.

The cells which contain the noble gases, buffer gases, and Rb are made of aluminosilicate glass (Corning 1720). This glass is used because the wall relaxation times for ^{3}He are found to be much longer—greater than 40 h—than cells made with borosilicate (Pyrex) glass in which the maximum observed ^{3}He times are about 2 h.[3,7] Wall relaxation times for ^{21}Ne and ^{129}Xe are shorter, i.e., 1–2 h, and are similar for the two types of glass. The cells are in the shape of spheres, with diameter 1.5 cm and of cylinders with 1.5-cm diameter and varying heights. The cylinders are used in the measurement of quadrupole splitting in ^{21}Ne described in more detail below. The cells are mounted on a "tree" with four to six cells per tree. They are prepared by ultrasonic cleaning with water and methanol and are attached to a hydrocarbon-free, ion-pumped, vacuum system. They are baked at 400 °C for at least 12 h and evacuated to a base pressure of less than 10^{-7} Torr. Natural Rb is then distilled with a flame and introduced into the cells followed by about 60 Torr of N_2 and the noble gases. The N_2 is necessary to quench trapping of resonant radiation by the high-density alkali-metal vapor.[2,3] All cells contain ^{3}He and either ^{21}Ne or

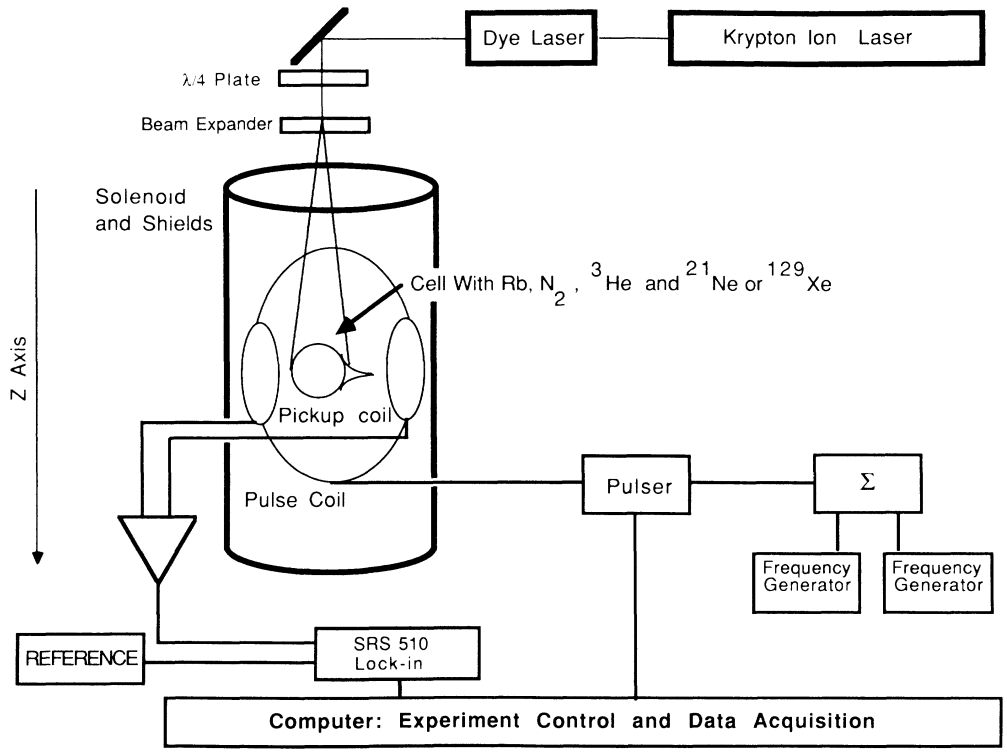

FIG. 1. Experimental overview. The major components are the laser system, the cell containing the noble gases, the precision solenoid, the NMR coils, and the acquisition and control electronics.

^{129}Xe.

The cells are placed in an oven which is integrated with the NMR coils. The oven is heated by hot air to a temperature of about 150 °C at which the Rb density[8,9] is 10^{14} cm^{-3}. At this Rb density, the polarization rates are sufficiently large to provide several percent polarization of ^{3}He and greater than 30% polarization of ^{21}Ne or ^{129}Xe after 1 h of optical pumping. The resulting free precession signals have amplitudes of 2–100 μV.

The magnetic field, of magnitude up to 3 G, is produced by a pair of coaxial solenoids inside a three-layer μ-metal shield. The solenoids are wound on coil forms of 6065-T6 aluminum alloy into which left-handed and right-handed threads of different depth are cut. The threads are provided to guide the two layers of windings on each solenoid and to insure uniform pitch (turns per unit length) over the 1.2-m length. After the threads were cut, the coil forms were etched to remove burrs and hard anodized to provide an insulating layer. The inner and outer solenoids are arranged so that the number of turns per unit length (12 and 6.5 turns per inch, respectively) is inversely proportional to the cross-sectional area, and equal but opposite currents flow through each. The external dipole moment of the pair is consequently small and most of the magnetic flux is returned between the two solenoids and not through the μ metal. The length of the two solenoids could be adjusted so that the second derivative of the magnetic field as a function of z, the axial coordinate, vanishes. However, for long solenoids this condition is nearly satisfied when the two have equal length.[10] The profile of the magnetic field is determined by the current density in the windings and the boundary conditions imposed by the presence of the μ-metal. Small coils provided a correction field that is empirically trimmed, by maximizing the free precession coherence time, so that the gradient of the magnetic field is less than 10^{-5} G cm. The μ-metal shields are easily magnetized by thermal or mechanical shock and by magnetic transients. The shields are demagnetized by a computer-controlled power supply with the two solenoids connected so that their fields are parallel. The maximum field produced, 30 G, is sufficient to saturate the entire magnetic shield. The average value of the magnetic field during demagnetization (the offset) is crucial. This offset is controlled to 10^{-4} G. The demagnetization procedure takes about 5 min and allows the uniformity to be reproduced repeatedly. The current for the solenoid is provided by a high-precision current source, built in our labora-

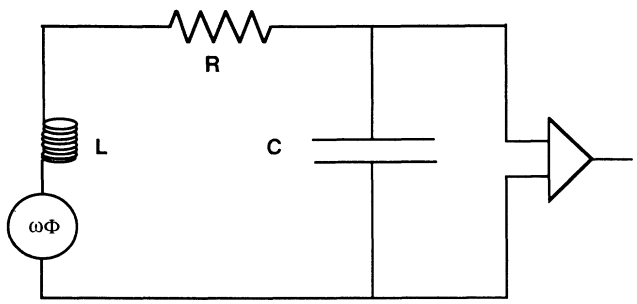

FIG. 2. Effective electrical circuit formed by the pickup coil.

tory, which has peak-to-peak variations less than 1×10^{-5} A. This current source can be controlled by a magnetometer based on Rb or ^{4}He to further reduce the contribution to the magnetic field noise.

The atoms in the cell are polarized along the z axis. A pulse of oscillating magnetic field directed along the y axis is then provided which rotates the magnetization due to each species by a small angle θ, which is typically 10°. The oscillating magnetic field is the sum of sine waves at each resonant frequency of the species present. For example, with ^{3}He and ^{21}Ne at 3 G, the two sine waves have frequencies of 9720 and 1008 Hz. The amplitudes are adjusted to provide the desired angle of rotation and optimum signal. The magnetization for each species **M** can be thought of in terms of two components, longitudinal M_z and transverse M_T. The longitudinal component has a smaller magnitude ($M\cos\theta$) than the original magnetization but identical relaxation time (T_1). The transverse component of initial magnitude $M\sin\theta$ precesses about the magnetic field with angular frequency $\omega=2\pi\gamma\,|\,\mathbf{B}\,|$ and has relaxation time T_2.

The precessing magnetization of each species induces a voltage in the pickup coil which is part of the circuit modeled in Fig. 2. The magnitude of the induced voltage for each species is (in V)

$$V_S=\omega\Phi\rho(\omega)\ . \tag{1}$$

Φ is the flux through the N turns of the pickup coil of area A, $\Phi=M_\phi NAq$, where q is a geometric factor which, in our experiment, is of order 0.1. $\rho(\omega)$ is the response of the circuit shown in Fig. 2,

$$\rho(\omega)=\frac{X_C}{[R^2+(X_L-X_C)^2]^{1/2}}\ . \tag{2}$$

X_L and X_C are the customary inductive and capacitive reactances. Note that for $X_L=X_C$, the resonance condition, $\rho(\omega)=\omega L/R=Q$, the quality factor of the circuit. The pickup coil is connected by low-capacitance cable to a preamplifier with a gain of 500–1000. The noise in the pickup-coil circuit is the combination of Johnson noise, preamplifier voltage noise, and current noise. This can be written

$$V_N=\sqrt{4kTfR\,(\Delta_{\rm BW})}\ , \tag{3}$$

where f is the noise factor of the circuit, and $fR=1000$ Ω is typical. The bandwidth ($\Delta_{\rm BW}$) is limited by the coherence time τ (the time constant for decay of M_T) and $\Delta_{\rm BW}\geq1/\tau$.

Time-domain signals are processed by mixing the preamplifier signals with a fixed reference frequency using linear sine-wave mixers provided in the SRS-510 lock-in amplifiers, as shown in Fig. 1. The reference signals are nearly equal to the precession frequencies, and the resulting beat frequencies are 0–1 Hz. The lock-in amplifier also provides low-pass filtering at the output, which limits the bandwidth of the mixer output. The lock-in outputs are digitized by ADC's (Data Translation DT2805) interfaced to the computer (PC-AT type). An example is shown in Fig. 3 of the beat frequency produced by mixing a 9670-Hz reference derived from a 10-MHz oven-stabilized quartz-crystal oscillator with the signal from the precessing ^{3}He. The Fourier transform of the data from this 1024-s sample is also shown in Fig. 3. The structure and width of the frequency-domain data show that the ^{3}He frequency varies due to the instability of the magnetic field, which has peak-to-peak variations of 10^{-5} G. In order to realize the precision possible with the polarized noble-gas atoms, this must be attenuated by several orders of magnitude with the techniques described in Sec. III.

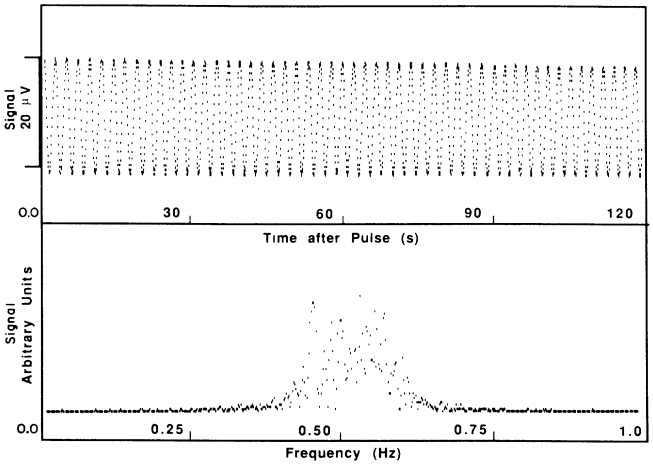

FIG. 3. Data from precessing ^{3}He. Top: time-domain data (beats are produced by mixing the signals from precessing ^{3}He with a fixed-frequency reference). The sample rate is 16 per second. Bottom: Fourier transform of 1024-s data sample. The resolution is 10^{-3} Hz.

The time-domain data show a finite value of τ, the coherence time of the signal. There are three contributions to decay of coherence: wall relaxation of M_T, dephasing of atomic spins as they diffuse through the inhomogeneous magnetic field, and damping due to the power dissipated in the pickup-coil circuit. The total rate of decay of coherence is the sum of the three rates

$$\frac{1}{\tau}=\frac{1}{T_W}+\tfrac{8}{175}(2\pi\gamma\nabla B_z)^2\frac{R^4}{D}+\frac{2\pi\gamma M_T qQ\dfrac{\omega}{\omega_0}}{1+\left[\dfrac{X_L-X_C}{R}\right]^2}\ , \tag{4}$$

where T_W is the relaxation time for spins due to interaction with the cell wall, ∇B_z is the gradient of the z component of **B**, R is the cell radius, and D is the diffusion constant, 1.2 $\mathrm{cm^2\,s^{-1}}$ for the pressure in our cells. The contribution due to ∇B_z arises from diffusion of spins which slows dephasing.[11] This magnetic-field-gradient dependence is an aproximation that is valid for the pressures and field gradients in our experiments and which we have confirmed by measurement. The dependence of τ on magnetic field inhomogeneity is discussed in detail by Cates *et al.*[11] The last term in Eq. (4) is the relaxation rate due to the power dissipated in the pickup coils and

can be made small by detuning the coil resonant frequency (ω_0) from the precession frequency (ω). This has the trade-off that V_S is reduced. The optimum relation of R, L, and C is realized by making $R \ll X_L \ll X_C$ and adjusting the number of turns and wire diameter of the pickup coils to satisfy this. With $\nabla B_z = 10^{-5}$ G cm^{-1} and $R = 0.75$ cm, the relaxation rate of the ^{3}He component of M_T due to magnetic field inhomogeneity is 1/(1200 s). For ^{21}Ne and ^{129}Xe the contribution due to magnetic field inhomogeneity is less due to the smaller values of γ, and $1/T_W$ is the dominant contribution to the transverse relaxation rate.

A special situation arises when the damping term is dominant in the coherence decay rate given in Eq. (4). In this case the current induced in the pickup coil produces an oscillating magnetic field which can rotate the magnetization further. The resulting increase in M_T leads to a larger induced current and a greater rate of rotation of the magnetization, etc. This possible cascade is gain, and can lead to "maser" amplification first observed for ^{3}He by Robinson and Myint.[12,13] The gain of the maser is maximum when the phase shift between the precessing magnetization and the induced current is $\pi/2$, that is, when the precession frequency is equal to the pickup-coil resonant frequency. Strong coupling can lead to a precession frequency shift[14] which must be avoided. The condition that $R \ll X_L \ll X_C$ suppresses the coupling and minimizes this frequency shift.

III. MAGNETOMETRY AND SIGNAL PROCESSING

The stability of $|\mathbf{B}|$ is the dominant limitation to the precision of our techniques. We have developed two types of magnetometry using ^{3}He, which effectively attenuate the magnetic field noise by 3 to 4 orders of magnitude. The first technique, used in measurement of frequency shifts due to dipole couplings, extracts the ratio of precession frequencies. The second technique, used in extracting quadrupole splitting, detects the beat frequency between precessing ^{21}Ne and a reference signal derived from the precessing ^{3}He, which tracks $|\mathbf{B}|$. In both cases the ^{3}He and second species are in the same cell and sample the same average magnetic field during the measurement.

A. Dipole couplings: The ratio measurement

Dipole couplings lead to a shift of the frequency. For example, in the search for a permanent atomic electric dipole moment, the interaction of a ^{129}Xe atom (or a ^{3}He atom) with parallel magnetic field ($\mathbf{B}$) and electric field ($\mathbf{E}$) gives rise to a precession frequency

$$\nu_{129} = \mathbf{s}\cdot\left[\frac{\mu_{129}}{hI_{129}}\mathbf{B} + \frac{d_{129}}{hI_{129}}\mathbf{E}\right], \tag{5}$$

where $\mu\mathbf{s}$ is the magnetic moment, $d\mathbf{s}$ is the permanent electric dipole moment of the atom, and I_{129} is the nuclear spin, which is 1/2 for ^{129}Xe. The precession frequency will change when the electric field is flipped between parallel and antiparallel to the magnetic field. The ratio of this frequency to the precession frequency of ^{3}He is

$$\frac{\nu_{129}}{\nu_3} \approx \frac{\mu_{129}}{\mu_3}\left[1 + \frac{\mathbf{E}\cdot\mathbf{B}}{B^2}\left[\frac{d_{129}}{\mu_{129}} - \frac{d_3}{\mu_3}\right] + O(d^2)\right]. \tag{6}$$

For the atomic electric dipole moments, d_3 is expected to be smaller than d_{129} by a factor of at least $(\frac{54}{2})^2$. The ratio of frequencies given in Eq. (6) is sensitive to the magnitude of $\mathbf{B}$ only in the term proportional to d/μ, which is much less than one. We therefore effectively eliminate magnetic field noise at frequencies within the bandwidth of the frequency counters. As shown below, this bandwidth can be made sufficiently large, at the cost of frequency resolution, to include all frequencies at which the magnetic field noise is significant.

A potential problem in the electric-dipole-moment work is the possibility that leakage currents flow and give rise to a contribution to $\mathbf{B}$ which is correlated with the sign of $\mathbf{E}\cdot\mathbf{B}$. This effect would give rise to an additional term in ν of value $\mathbf{s}\cdot(\mu\epsilon\mathbf{E})$, where we have written the correlated contribution to $\mathbf{B}$ as $\epsilon\mathbf{E}$. If we neglect the electric-dipole-moment contribution, Eq. (6) becomes

$$\frac{\nu_{129}}{\nu_3} \approx \frac{\mu_{129}}{\mu_3}\left[1 + \frac{\epsilon\mathbf{E}\cdot\mathbf{B}}{B^2}\left[\frac{\mu_{129}}{\mu_{129}} - \frac{\mu_3}{\mu_3}\right]\right] = \frac{\mu_{129}}{\mu_3}. \tag{7}$$

The ratio is independent of $\mathbf{E}$. In fact, all false effects arising from coupling of magnetic fields to the atoms magnetic moments are absent in the ratio of frequencies.

Frequency shifts can also arise due to hyperfine coupling to the Rb and the effects of magnetic impurities in the glass cell walls. If Rb is present in the vapor, it will be polarized by spin exchange with the noble-gas atoms. This process is weak compared to laser optical pumping, but can lead to several percent Rb polarization in the presence of polarized ^{129}Xe (Ref. 5). The polarized Rb gives rise to an effective magnetic field at the noble-gas-atom's nucleus, which is a function of Z and leads to a shift proportional to the density of Rb vapor which is different for each species.[15] This effect can be suppressed by cooling the cell to remove the Rb from the vapor. Furthermore, this effect is not correlated with the relative orientation of $\mathbf{E}$ and $\mathbf{B}$. Magnetic impurities in the cell walls also lead to shifts that are different for different species since the sticking time varies. This effect is also uncorrelated with $\mathbf{E}\cdot\mathbf{B}$.

The frequencies are measured with the system shown in Fig. 4. The output of the preamplifier is distributed to two phase-locked loops (PLL). Each PLL has a voltage controlled oscillator (VCO) which is limited to ± 30 Hz around the precession frequency. The VCO produces a square wave which, divided by N, gates a scalar. The scalar counts the number of pulses from the 10-MHz clock corresponding to N periods. The ratio of N for ^{129}Xe and ^{3}He is equal to the inverse of the ratio of precession frequencies so that the scalars are read by the computer at the same rate. The resolution ($\delta\nu$) and bandwidth (Δ_{BW}) of this frequency measurement are

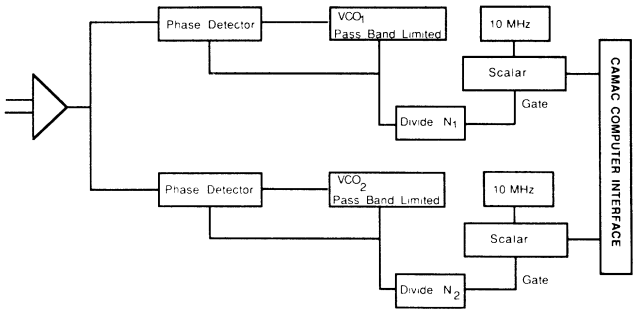

FIG. 4. System used to extract the ratio of precession frequencies. The phase detectors are Ithaco 393 vector lock-in amplifiers.

$$\delta\nu=\frac{\nu^2}{(N)10\ \text{MHz}}\ ,$$
$$\Delta_{\text{BW}}=\frac{\nu}{2N}\ . \tag{8}$$

The frequency resolution and bandwidth of this measurement technique can be compared to those for the Fourier-transform technique. For example, with a 0.1-s data-collection interval and $\nu=1$ kHz ($N=100$), the resolution is 10^{-3} Hz and the noise bandwidth is 5 Hz. For the Fourier-transform technique this resolution and bandwidth would require a 1000-s data-collection interval and a 10-Hz data-acquisition rate, i.e., 10 000 samples.

B. Quadrupole splittings

In an atom or nucleus with spin greater than $\frac{1}{2}$, quadrupole splitting can arise. ^{21}Ne has nuclear spin $I_{21}=\frac{3}{2}$, and the quadrupole splitting of the precession frequency spectrum appears as three lines as shown in Fig. 5. The three frequencies will be apparent in the beats produced by mixing the ^{21}Ne signals with a reference signal derived from the ^{3}He. The reference signal is produced with the system shown in Fig. 6. In this setup a PLL is used to lock the VCO to a frequency 1000 times the ^{3}He precession frequency. The VCO output is then divided by 9649. The ratio of the precession frequencies of ^{21}Ne to ^{3}He is

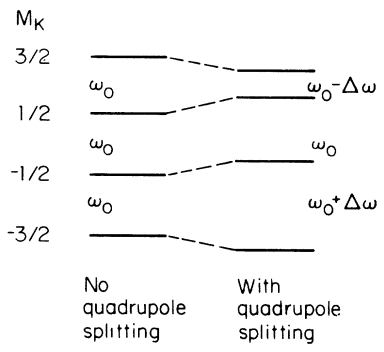

FIG. 5. The effect of a quadrupole splitting on the NMR lines of ^{21}Ne.

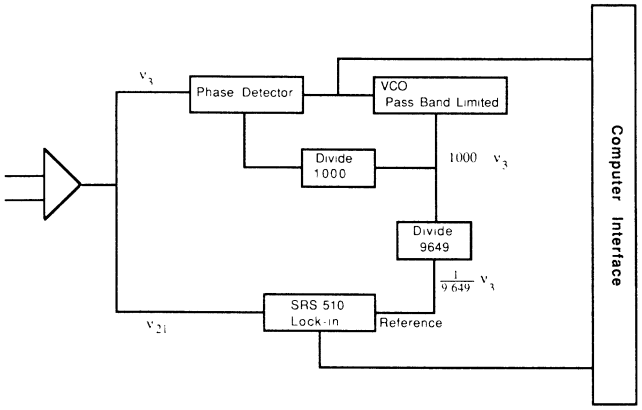

FIG. 6. The system used to determine the frequency spectrum of ^{21}Ne with ^{3}He magnetometry.

nearly 1/9.649. The resulting reference signal is within 0.1 Hz of the ^{21}Ne precession frequency and the beat frequency is

$$\nu_{\text{beat}}=\left[\frac{\mu_{21}}{hI_{21}}-\frac{1}{9.649}\frac{\mu_3}{hI_3}\frac{G}{1+G}\right]|\mathbf{B}|\ , \tag{9}$$

where G is the gain of the PLL. For magnetic field noise frequencies at which $G\gg1$, the noise is attenuated by the ratio $\nu_{\text{beat}}/\nu_{21}$, which is 10^{-4} for $\nu_{21}=1$ kHz. For frequencies at which the PLL gain is less than 1, there is no attenuation of magnetic field noise.

Figure 7 shows the beat frequency derived with this technique along with the Fourier transform of ν_{beat} for the entire 1024-s run. The Fourier transform is well fit by a single-frequency Lorentzian with width 1×10^{-3} Hz, consistent with $T_2=1500$ s. The time-domain data have been fit to a single frequency spectrum. For the 1024-s

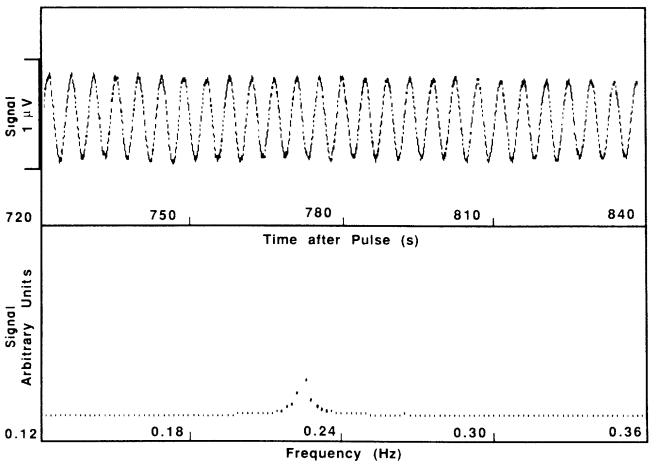

FIG. 7. Data from precessing ^{21}Ne. Top: time-domain data (the beat frequency of precessing ^{21}Ne and a reference frequency derived from precessing ^{3}He). The sample rate is 16 per second. Bottom: Fourier transform of the 1024-s data sample. The resolution is 10^{-3} Hz.

run, the frequency is determined with a precision of 4×10^{-7} Hz. The Fourier-transform data should be compared to those of Fig. 2 which shows, for the same run, the variation of the ^{3}He precession frequency due to magnetic field noise.

IV. SUMMARY: THE APPLICATIONS

The dipole- and quadrupole-measurement techniques are to be applied, respectively, to the measurement of magnetic and electric dipole moments and to the search for violation of local Lorentz invariance. The precision possible with each technique is only part of the story. It is essential to have a measure of the fake effects that will appear in order to minimize them and correct for them. In the case of the electric-dipole-moment measurement, the major fake effects arise from magnetic field contributions due to leakage currents. As shown in Eq. (7), this effect is not present in the ratio of precession frequencies. Similar measurements have been reported, the most recent results by Vold *et al.*[16] A major distinction between the previous experiments and our experiment is the use of the ^{3}He magnetometry.

Modern searches for local Lorentz invariance violation have used trapped ions[17] and optically pumped Hg ions.[18] For our measurement of quadrupole splittings, the greatest precision will be possible if the three lines can be separately resolved. In our current investigations with nearly spherical cells, the data are best fit with a single frequency and only an upper limit for $\Delta\omega$ can be extracted. Recently Wu *et al.* have shown that enhanced quadrupole splitting in ^{131}Xe arises in cylindrical cells with pancakelike quadrupole asymmetry.[19] We have recently produced cells of this shape with the hope of inducing an observable splitting.

The signal of Lorentz invariance violation is a modulation of $\Delta\omega$ that is proportional to $P_2(\cos\beta)$, where β is the angle between the quantization axis and a postulated preferred direction. The signal is therefore correlated with sidereal time, and any diurnal or semidiurnal variations of $\Delta\omega$ fake Lorentz invariance violation. It is essential to confirm the stability of $\Delta\omega$ and to search for correlations with room temperature, ambient magnetic field, floor vibrations caused by traffic, etc. A significant fraction of the time spent on the experiment must be devoted to such studies. Our techniques provide high precision in short runs. This allows devotion of a significant fraction of time to study of systematic effects.

ACKNOWLEDGMENTS

We wish to thank G. Cates and R. Loveman for useful discussions. This material is based upon work supported by a National Bureau of Standards Precision Measurement Grant, a grant from the Research Corporation, and the National Science Foundation under Grant No. PHY-8605081. One of us (E.R.O.) acknowledges the support of the National Science Foundation. One of us (T.E.C.) acknowledges the support of the Alfred P. Sloan Foundation.

[1]M. Bouchiat, T. Carver, and C. Varnum, Phys. Rev. Lett. **5**, 373 (1960).
[2]T. E. Chupp, M. E. Wagshul, K. P. Coulter, A. B. McDonald, and W. Happer, Phys. Rev. C **36**, 2244 (1987).
[3]T. E. Chupp and K. P. Coulter, Phys. Rev. Lett. **55**, 1074 (1985).
[4]C. H. Volk, J. G. Mark, and B. C. Grover, Phys. Rev. A **20**, 2381 (1979).
[5]X. Zeng, Z. Wu, T. Call, E. Miron, D. Schreiber, and W. Happer, Phys. Rev. A **31**, 260 (1985).
[6]M. Pitt *et al.*, Bull. Am. Phys. Soc. **32**, 1034 (1987).
[7]W. A. Fitzimmons and G. K. Walters, Phys. Rev. Lett. **19**, 943 (1967).
[8]T. Killian, Phys. Rev. **27**, 578 (1926).
[9]Z. Wu, M. Kitano, W. Happer, M. Hou, and J. Daniels, Appl. Opt. **25**, 4483 (1986).
[10]B. Heckel and E. M. Purcell provide useful suggestions relating to the magnet design.
[11]G. D. Cates, S. Shaefer, and W. Happer, Phys. Rev. A **37**, 2877 (1988).
[12]H. G. Robinson and M. T. Myint, Appl. Phys. Lett. **5**, 116 (1964).
[13]M. T. Myint, Ph.D. thesis, Harvard University, 1966.
[14]A. Yariv, *Quantum Electronics* (Wiley, New York, 1975), p. 180.
[15]B. C. Grover, Phys. Rev. Lett. **40**, 391 (1978).
[16]T. G. Vold, F. J. Raab, B. Heckel, and E. N. Fortson, Phys. Rev. Lett. **52**, 2229 (1985).
[17]J. D. Prestage *et al.*, Phys. Rev. Lett. **54**, 2387 (1985).
[18]S. Lamareaux *et al.*, Phys. Rev. Lett. **57**, 3125 (1986).
[19]Z. Wu, W. Happer, and J. Daniels, Phys. Rev. Lett. **59**, 1480 (1987).